Vietnam Journal of Science and Technology ***60*** *(2) (2022) 203-215*

doi:10.15625/2525-2518/16040

INVESTIGATING THE PERFORMANCE OF FULL-CELL USING $NaFe_{0.45}Cu_{0.05}Co_{0.5}O_2$ CATHODE AND HARD CARBON ANODE

Hoang Van Nguyen[1, 3], Minh Le Nguyen[1, 2], Phuong Hue Tran[1, 2], Man Van Tran[1, 2, 3], Phung My Loan Le[1, 2, 3, *]

[1]*Applied Physical Chemistry Laboratory (APCLab), University of Science, VNUHCM*

[2]*Department of Physical Chemistry, Faculty of Chemistry, University of Science, VNUHCM*

[3]*Vietnam National University Ho Chi Minh City, VNUHCM*
227 Nguyen Van Cu street, Ward 4, District 5, Ho Chi Minh City, Vietnam

[*]Email: *lmlphung@hcmus.edu.vn*

Received: 30 April 2021; Accepted for publication: 10 March 2022

Abstract. The reliable candidates for practical Na-ion batteries can be found among various layered structure sodium transition metal oxides because of the high working voltage and high specific capacity. However, hard carbon anode remains an obstacle to increasing the energy density of the cell because of its high irreversible capacity. In this work, a full-cell was assembled using the synthesized cathode $NaFe_{0.45}Cu_{0.05}Co_{0.5}O_2$ (NFCCu) and hard carbon (HC) as the anode. We evaluated methods aimed at improving the performance of full-cell including i) Presodiating HC by discharging to 0.1 V in half-cell; ii) Presodiating HC by contacting with Na metal; iii) Activating by low current charging at an initial rate of C/20; and iv) Constant current charging to a cutoff voltage of 3.95 V then holding the voltage for 6 hours. The full-cells were characterized by cycle testing at a rate of C/10. Galvanostatic profile of NFCCu at C/10 rate in the voltage range of 2.5 - 4.0 V exhibited a specific initial capacity of 131 $mAh.g^{-1}$. In practical full-cell of HC||NFCCu, a reversible capacity of 87.5 $mAh.g^{-1}$ was obtained. The full-cells were characterized by the given methods. The results showed that the cell being charged by low current density did not exhibit feasible work and its capacity was low. Cell (iv) displayed an improvement in capacity while cell (i) and cell (ii) are both better in terms of Coulombic efficiency. In summary, the capacity and capacity retention of the cells treated with the suggested methods still did not show an attractive improvement as compared to that obtained by the cell using pure HC. A feasible solution is that the process should be optimized and the quality of the anode electrode maintained prior to assembly of the full-cell.

Keywords: full-cell, hard carbon, Na-ion batteries, $NaFe_{0.45}Cu_{0.05}Co_{0.5}O_2$, presodiated.

Classification numbers: 2.8.2, 2.9.4.

1. INTRODUCTION

Lithium-ion batteries (LIBs) have played a vital role in the success of electric-electrical products for decades and even in the future. However, poor reserves in the earth's crust and

increasing prices of lithium compounds have seriously hindered the further development and application of LIBs in upcoming applications, especially for large-scale energy storage systems and electric vehicles [1 - 3]. Therefore, much attention has turned to sodium-ion batteries (SIBs) since the sodium resources are readily available, abundant, and inexpensive, this is perfectly suited for large-scale production [2, 4 - 6].

Layered structure sodium transition metal oxides (Na_xTMO_2) have received much attention as a potential candidate for high-performance SIBs because their electrochemical properties are flexibly adjusted by changing the component elements. Researches on electrode materials for SIBs have been inspired by LIBs' counterparts, typically electrode structure and composition. Although the state-of-the-art LIBs use ternary systems with $LiNi_{1/3}Mn_{1/3}Co_{1/3}O_2$ as a representative example and the newly developed Ni-rich material $LiNi_{0.8}Mn_{0.1}Co_{0.1}O_2$, the development of binary systems on SIBs is also attractive, especially the Mn-based and Fe-based systems which are interesting because of their abundant and inexpensive resources [7 - 10].

Replacing metal in transition metal octahedral slabs has been demonstrated as an effective strategy to enhance the electrochemical properties of electrode materials. Fe can be incorporated into various electrode compositions to replace toxic and expensive elements like Co, Ni [11 - 16] and reduce the cost of the electrode. The partial substitution of Co by Fe in $NaFe_{0.5}Co_{0.5}O_2$ has enhanced the capacity and rate capability thanks to the synergic effect of Fe và Co ions. The material delivered a high specific capacity of about 160 $mAh.g^{-1}$ and superior rate capability that delivered 80 $mAh.g^{-1}$ at 30C [14]. Mg substitution has been conducted to enhance structure stability and long cycling stability [17]. The dopants can be electrochemically active or inactive elements such as Al, Mg, Zn, Cu, Ti, etc. [18 - 21]. In our previous work, we introduced Cu-substitute for Fe in $NaFe_{0.45}Co_{0.5}Cu_{0.05}O_2$ obtained by a solid-state reaction at 900 ^oC, creating a promising, low cost and high-performance electrode for SIBs because of its high performance in half-cell test with a high working potential of above 3 V, high capacity of about 131 $mAh.g^{-1}$ and stable cycling over 200 cycles [22].

For the anode, the use of carbonaceous materials is highly acceptable to reduce the cost of the batteries. Among various classes in carbonaceous, hard carbon (HC) is considered a star because it delivers a practical specific capacity of above 250 - 350 $mAh.g^{-1}$ which is comparable to graphite anode in LIBs and exhibits low voltage plateaus and long-term durability [23 - 25]. Furthermore, the main synthesized route of HC by pyrolysis of organic materials/biomass which was available everywhere made it the anode of choice for practical SIBs. The electrochemical properties of HC depend on the microstructure related to heat treatment and electrolytes. The obstacle of HC is related to its low initial Coulombic efficiency [26]. The obstacle, however, can not prevent our tremendous efforts to assemble full-cell SIBs from our synthesized cathodes and the available HC anode. In particular, electrode materials play a vital role in the performance of the full-cell and the cathodes should have high working potential to increase the output voltage of the cell.

In this work, full-cell SIB was assembled using $NaFe_{0.45}Cu_{0.05}Co_{0.5}O_2$ and commercial HC as the cathode and the anode, respectively, to evaluate the effectiveness of presodiated methods of hard carbon anode and the charging mode to the performance of the full-cell. The use of $NaFe_{0.45}Cu_{0.05}Co_{0.5}O_2$ and HC is desirable to enhance the durability and voltage of the full-cell.

2. MATERIALS AND METHODS

2.1. Materials

Na_2CO_3 (≥ 99.9 %, Merck), $Fe(C_2O_4).6H_2O$ (≥ 99 %, Merck), $Co(NO_3)_2.6H_2O$ (≥ 95 %, Sigma-Aldrich), and $Cu(OAc)_2$ (≥ 98 %, Sigma-Aldrich). All chemicals were used without further purification.

2.2. Synthesis of cathode material

The synthesis of $NaFe_{0.45}Cu_{0.05}Co_{0.5}O_2$ material (hereafter denoted as NFCCu) through a solid-state reaction was previously reported by our group [22]. Typically, the reactants of Na_2CO_3, $Fe(C_2O_4).6H_2O$, $Co(NO_3)_2.6H_2O$, and $Cu(OAc)_2$ in stoichiometry were thoroughly mixed with about 1 mL of distiled water then heated at 400 ^oC for 12 hours in the air followed by sintering at 900 ^oC for 24 hours in the air. Finally, the sample was directly moved to the argon-filled glove box for grinding and storage.

Phase component and structure were analyzed by XRD on a D8 Advance (Bruker) diffractometer with 0.02^o/step/0.25 seconds. The Rietveld method is implemented on Material Studio (2017) software.

Surface morphology and particle size are determined using Scanning Electron Microscopy (SEM) analysis (FESEM SU3500, Hitachi) coupled with Energy-Dispersive X-ray Spectroscopy (EDS) detector for element determination. Atomic Absorption Spectroscopy (AAS) was used to determine the chemical formula.

2.3. Electrode preparation and cell assembly

The cathode electrode was prepared by a doctor-blade technique. The slurry made from active material NFCCu, conducting carbon C65, and the binder poly(vinylidene fluoride-co-hexafluoropropylene) (PVDF-HFP) were mixed at a weight ratio of 80:15:5 and 90:5:5 in N-methylpyrrolidone (NMP) solvent for half-cell and full-cell, respectively, and then coated on a technical aluminum film. The film was dried at 110 ^oC for 12 hours in an argon-filled glove box before being cut into 12 mm diameter electrode discs matching the diameter of the CR2032 coin-cells. The anode electrode made of hard carbon (HC), carbon C65, and PVDF-HFP at a weight ratio of 90:5:5 was prepared by the same process as the cathode.

Half-cell was assembled using an as-prepared electrode disc and sodium metal as the counter separated by two Whatman glass microfibers (GF/F). Full-cell was assembled using the prepared cathode electrode and the anode electrode separated by a Whatman glass microfiber (GF/F). The electrolyte was 1 M $NaClO_4$ in propylene carbonate (PC) with 2 % fluoroethylene carbonate (FEC) as an additive.

2.4. Cell characterization

The electrochemical characterization of the materials was conducted on a multi-channel MPG2 apparatus (Biologic). Cycle tests were performed on half-cell at a constant current of C/10 and in a voltage range of 2.0 - 4.0 V for the cathode and 0.01 - 2.0 V for the anode. Typically, 1C = 237.7 $mAh.g^{-1}$ and 372.2 $mAh.g^{-1}$ were of the cathode and the anode, respectively, and 1C rate corresponding to the extraction of 1 sodium ion for 1 hour.

Presodiated HC anode was obtained via electrochemical and chemical methods to overcome the large irreversible capacity in the first discharge. In the electrochemical method, HC electrode was cycled in half-cell for 3 cycles, then interrupted at 0.1 V on the 4th discharge, and was denoted as pHC (presodiated hard carbon). In the chemical method, the HC electrode

was in direct contact with a slice of sodium metal for 30 minutes in the presence of an electrolyte and was denoted as cHC (chemically presodiated hard carbon).

The performance of full-cell was evaluated by constant current charge-discharge (CCC-CCD) testing over a voltage range of 1.0 - 3.95 V. The baseline charge-discharge mode (M1) including the CCC-CCD regime at C/10 rate for both charge and discharge sequences. Indeed, a regime including CCC-CVC-CCD was named M2 where CCC-CCD was interleaved with constant voltage charging (CVC) at 3.9 V for 6 hours. Another regime named M3 was the CCC-CCD regime at C/20 for the first cycle, then at C/10 for the following cycles.

3. RESULTS AND DISCUSSION

X-ray diffraction result of the synthesized NFCCu in Figure 1(a) exhibited high intensity, well-defined peaks, and low background baseline. Such these peaks in ascending order of 2θ degree well fitted to the lattice planes of (003), (006), (101), (012), (104), (107), (018) (110), and (113) of O3-type layered structure (PDF#01-073-2048) without any peak of impurity. Therefore, the XRD results indicated that the O3-NFCCu was obtained. The XRD pattern was refined based on the O3-type layered structure with hexagonal symmetry and R-3m space group, which yield a sufficiently small value of R_{wp} = 7.05 %, indicating a good consistency between the calculated pattern and the experimental pattern. The calculated lattice parameters were a = b = 2.9399 Å, c = 15.8884 Å and V = 118.93 $Å^3$, that were close to the previous reports [14, 17, 27]. Compared with unsubstituted $NaFe_{0.5}Co_{0.5}O_2$ [22], the introduction of Cu into the lattice shortens the average M–O bond length, inducing the shrinkage of the MO_6 octahedral and lattice volume as well.

SEM images of the synthesized material in Figure 1(b-c) showed irregular-shaped polygonal particles with the size of a few micrometers made up of the agglomeration of flaky particles with smaller dimensions. The particle size was not the matter for using as electrode material but the size distribution was quite large due to high-temperature treatment. Additionally, EDS analysis was carried out on the NFCCu sample as shown in Figure 1(d-i) to verify the presence of the elements in the material. The chemical formula calculated from the AAS result was $Na_{0.942}Cu_{0.065}$ $Fe_{0.381}Co_{0.555}O_{3.028}$ in relatively weak accordance with the nominal ratio of the precursors and the expected formula. Assuming that the sum of metals and oxygen is 100 %, the oxygen fraction was obtained by dividing the percentage of oxygen by the sum of the transition metals. However, the value is abnormal to layered structure compounds and may result from structural defects due to doping or cooling process.

Electrochemical properties of the NFCCu material were investigated in a half-cell configuration. As shown in Figure 1(j), the material displays a charge-discharge profile similar to that of the un-substituted $NaFe_{0.5}Co_{0.5}O_2$ sample, but the discharge curve is more stepper [14], possibly due to the effect of Cu substitution in the lattice. When the oxidation state of ions rose on charging, the inhomogeneous distribution of ions and defects with different sizes caused the substitute material to change from solid solution - of the pristine to phase transfer-like intercalation mechanism. The voltage jumping at around 3.2 - 3.4 V could be observed on charge and discharge curves. However, the charge-discharge curve remained the typical shape for over ten cycles and the capacity declined slightly. As seen in Figure 1(k), the material exhibited relatively good performance. The capacity is 131 $mAh.g^{-1}$ at the first discharge and 118 $mAh.g^{-1}$ at the 50^{th} discharge cycle with a retention of 90.07 %. The Coulombic efficiency (H %) is 92 % at the first cycle and remains at nearly 100 % for the following cycles, indicating a highly reversible charging and discharging process.

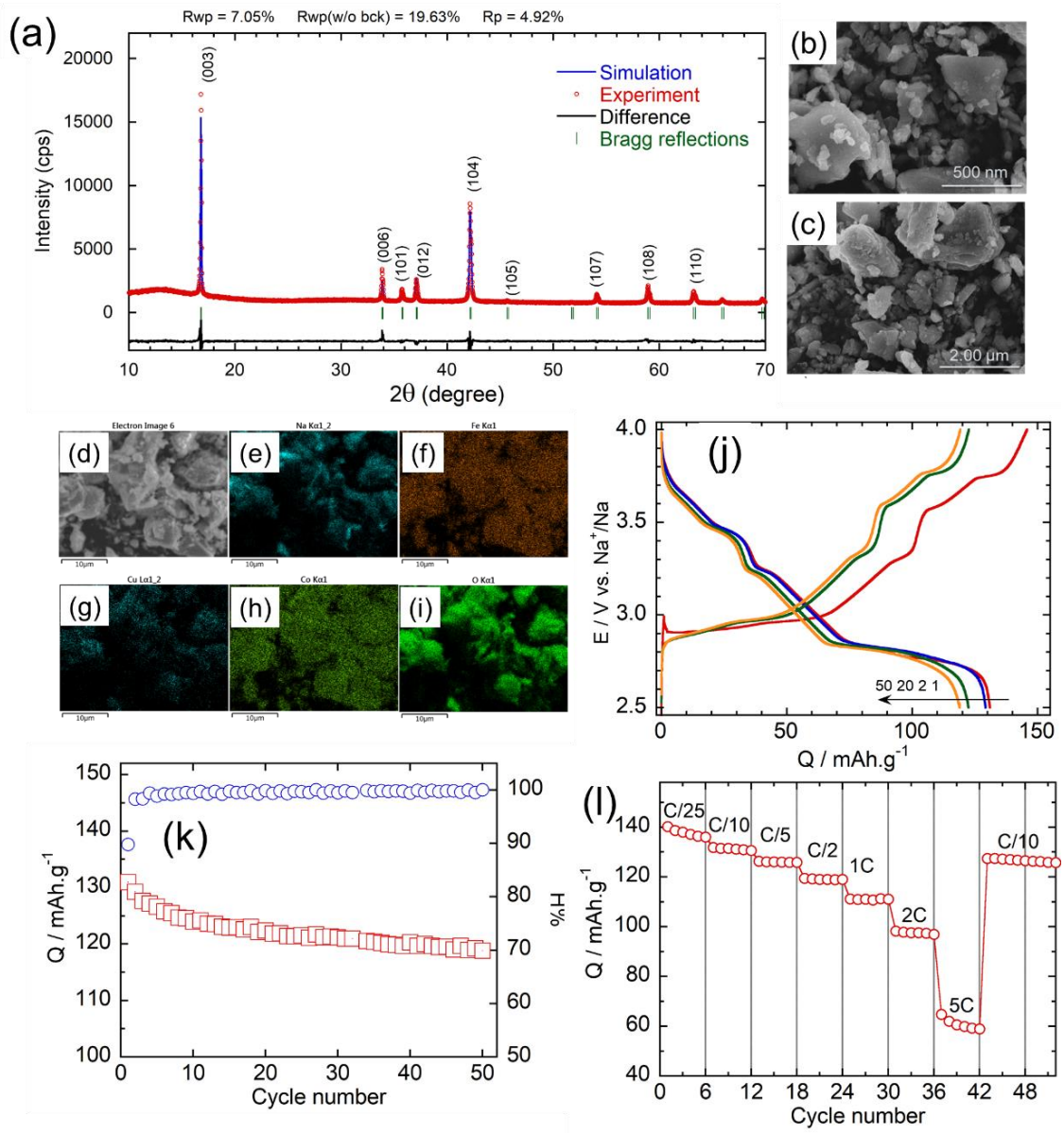

Figure 1. Structure, morphology and electrochemical performance of the synthesized $NaFe_{0.45}Cu_{0.05}Co_{0.5}O_2$ material. (a) X-ray diagram, (b-c) SEM images, (d-i) Element mapping results, (j) Charge/discharge curves at various cycles, (k) Evolution of capacity over cycle number and (l) rate capability.

Figure 1(l) shows the rate capability of NFCCu electrode when the applied current density varies from C/10 to 2C. The stable cycling was seen for every rate of charge-discharge. The highest capacity delivered is about 137 $mAh.g^{-1}$ at a rate as low as C/25. As the rate increases, the capacity decreases. The NFCCu material exhibits a reversible capacity of 131, 125, 119, 111, 97, and 59 $mAh.g^{-1}$ at discharge rates of C/10, C/5, C/2, 1C, 2C, and 5C, respectively. The capacity could recover 92 % of its original capacity when the rate returned to C/10 after forty cycles of the test. The electrochemical performance of NFCCu is improved as compared to that

of pristine $NaFe_{0.5}Co_{0.5}O_2$ synthesized by the same process [22], but a slight improvement could be obtained by Mg doping [17].

Besides, the performance of HC anode was also investigated in a half-cell. Hard carbon exhibited typical charge-discharge curves (Figure 2(a)) with a sloping region and a long flat plateau region, demonstrating two steps of sodium storage mechanism. The first discharging delivered a capacity of 338.4 $mAh.g^{-1}$ including the decomposition of the electrolyte solvent and sodium ions intercalated at irreversible sites between graphene layers [28], so a reversible capacity of about 255 $mAh.g^{-1}$ was obtained in the next charge with an initial Coulombic efficiency of 72.6 %. The capacity gradually decreases over cycles and remains 238.9 $mAh.g^{-1}$ at the 50th cycle as seen in Figure 2(b).

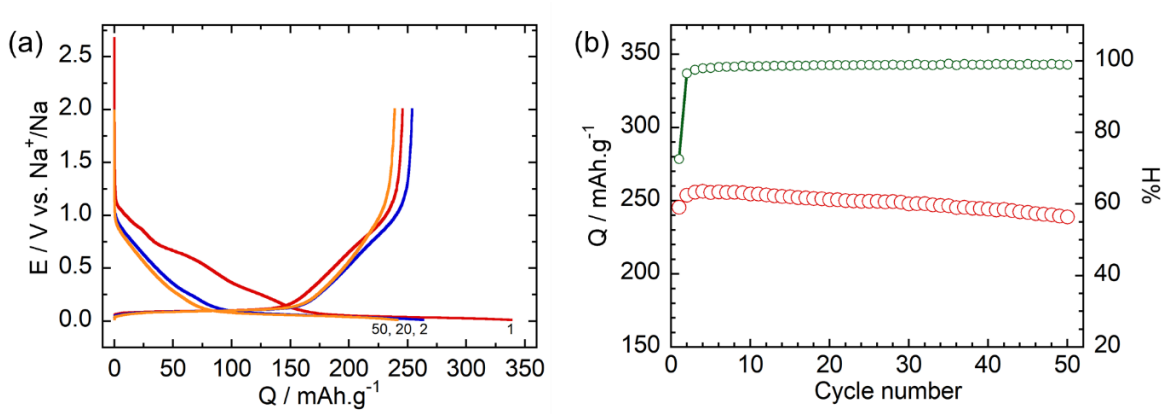

Figure 2. (a) Charge/discharge curves of hard carbon electrode at various cycles and (b) capacity and Coulombic efficiency during cycling.

Table 1. Performance parameters of full-cell in charge/discharge test.

Anode	Initial charge capacity ($mAh.g^{-1}$)	Initial discharge capacity ($mAh.g^{-1}$)	Initial Coulombic efficiency (%)	25th discharge capacity ($mAh.g^{-1}$)	Discharge capacity retention (%)
Pure HC	137.0	72.6	53.0	40.6	55.9
pHC	112.2	68.0	60.6	42.9	63.1
cHC	125.7	60.4	48.0	4.9	8.1

A full-cell SIB was fabricated by coupling the NFCCu cathode and pure hard carbon (HC) anode and the weight ratio of the active material of the cathode and the anode was optimized to be about 2.95. The charge-discharge profile of the SIB is shown in Figure 3(a). The voltage profile of the SIB is almost exactly the subtraction of the cathode and the anode. The long flat plateaus of the NFCCu electrode are almost seen on the first charge curve but sloping curves are seen in the next following cycles. The capacity of the cell at the first charge could be as high as the half-cell but nearly a half could be delivered by the cell at the next discharge as a result of the highly irreversible pure HC in the first cycle. The lack of sodium ion returning to the NFCCu electrode made it impossible to obtain a fully discharge state. The trend of capacity change is given in Figure 3(b). It can be seen that the capacity declines dramatically after about 15 cycles

then the decreased gradually with each cycle. The performance parameters of the cell are given in the second row of Table 1. After 100 cycles, the capacity of the full-cell decreases to 13.6 $mAh.g^{-1}$, and the capacity retention is 18.7 %.

In Figure 3(c), the voltage profile of the SIB using NFCCu coupled with HC which was presodiated in half-cell (pHC) demonstrates the same characteristics as the cell using pure HC. Additionally, a slight difference on the first charge curve was seen because the initial stage of pHC after presodiation and the pure HC is not the same. Figure 3(d) shows that the capacity of the cell decreases sharply within the first 10 cycles and then decreases slowly in the following cycles.

In Figure 3(e), as the initial stage of HC presodiated by direct contact with sodium metal (cHC) and pure HC is not the same, the first charge of the cell using NFCCu coupled with cHC exhibits a charge curve different from that of the cell using pure HC but close to the charge curve of NFCCu in half-cell with sodium metal anode, demonstrating that a solid electrolyte interface (SEI) is formed on the surface of HC. Moreover, the stacking graphene layers and holes in HC structure are filled with sodium ions when contacting. However, the capacity of the cell decreases significantly after the first cycle (Figure 3(f)) due to many reasons, such as mechanical cracking of the HC electrode, the capacity of the cathode, anode mismatches after being sodiated, thick SEI and surface contaminations due to electrolyte deposition of the HC anode through sodium contacting.

As can be seen in Table 1, the first capacity of the full-cell with presodiated HC is lower than that of the cell using pure HC due to the reasons as mentioned. Thus, only the pHC improves the ICE and capacity retention of the full-cell.

Because the presodiated methods involve the risk of electrode deformation, pure HC is highly preferred to be used as the anode for full-cell even though its low ICE reduces the gravimetric energy density.

Furthermore, the performance improvement and long cycle life of batteries depend not only on the efficiency of the anode, but also on the charging regime [29–31]. Thus, the charge regimes were investigated to see if they could improve the cycling stability of the full-cell. Figure 4 illustrates the performance of full-cells with various charge/discharge regimes and the results as listed in Table 2.

For comparison, the M2 method completely improves both capacity and ICE (Figure 4a)). A capacity of 90.6 $mAh.g^{-1}$ and ICE as high as 69.6 % were obtained (Table 2). It can be depicted from the results that the CVC sequence encourages time-limited reactions at the electrodes so that additional sodium ions can be extracted from the cathode and intercalated to the anode side. However, sustaining long periods at high cutoff voltages can encourage many side reactions such as electrolyte decomposition, self-reaction at the cathode/anode side, release of gases, etc, so that the capacity deterioration degree is even higher than that of the pure HC-anode full-cell (Figure 4(b), Table 2).

On the other hand, the full-cell applying the M3 method cannot work thoroughly (Figure 4(c), Table 2). The first charge curve is contributed by the flat voltage region and sloping voltage regions that are entirely different from the other cells. Furthermore, the flat voltage persisting for so long indicates that the cell cannot be charged, which may contribute to the continuous electrolyte composition to form the SEI layer at the anode side. Because the charge was used to reduce the electrolyte at the anode, the HC anode material was partially reduced and just accepted a small amount of sodium ion from the cathode, leading to the low capacity of the cell. The cell gradually lost its capacity over 50 cycles (Figure 4(d), Table 2).

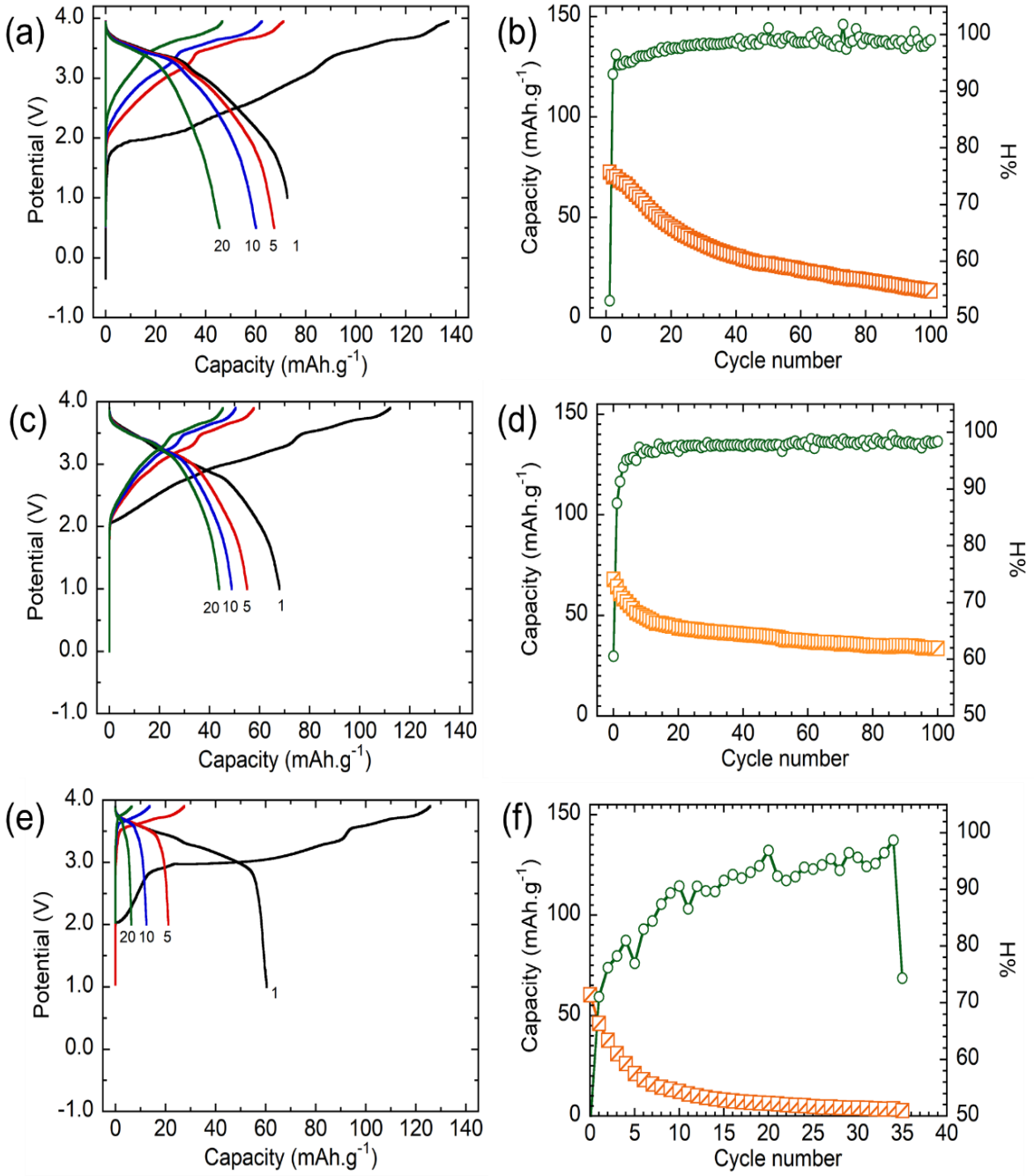

Figure 3. Charge/discharge curves of full-cell using pure HC (a), pHC (c) and cHC (e). Capacity and Coulombic efficiency versus cycle number of full-cell using pure HC (b), pHC (d), and cHC (f).

Table 2. Performance parameters of full-cell in charge/discharge test.

Method ID	Initial charge capacity ($mAh.g^{-1}$)	Initial discharge capacity ($mAh.g^{-1}$)	Initial Coulombic efficiency (%)	25th discharge capacity ($mAh.g^{-1}$)	Discharge capacity retention (%)
M1	137.0	72.6	53.0	40.6	55.9
M2	130.0	90.6	69.6	24.8	27.4
M3	101.7	27.7	27.2	15.3	55.2

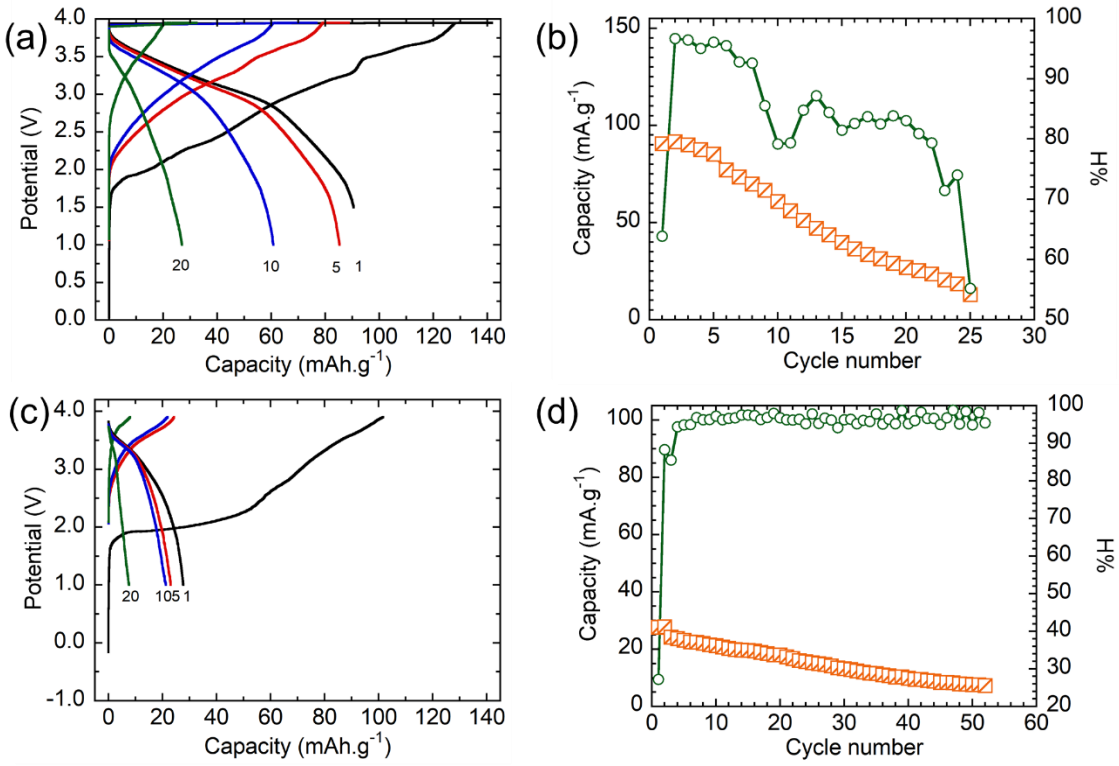

Figure 4. Charge/discharge curves (a) and Capacity and Coulombic efficiency versus cycle number (b) of full-cell using pure hard carbon in CCC-CCV-CCD mode. Charge/discharge curves (c) and Capacity and Coulombic efficiency versus cycle number (d) of full-cell using pure hard carbon in CCC-CCD mode with C/20 rate of charge/discharge in the first cycle.

The low ICE of the anode is the bottleneck of high-performance SIB that demands more mass loading at the cathode and reduces the energy density of the cell. Many efforts have been made to improve the capacity and ICE of HC by heat/chemical treatment, doping, and presodiation, etc. [4]. In this work, we evaluated many presodiation methods and charge/discharge regimes on the sodium-ion full-cell with the available electrode materials such as HC and NFCCu. All cells are assembled with a mass ratio of the cathode active material and

the anode active material of about 2.95 which is the optimized ratio to obtain the highest capacity of the full-cell using pure HC.

It is observed that the full-cell using pure HC exhibits fast capacity degradation which is due to irreversible reactions at the anode side because the NFCCu exhibited strong structure stability [22]. Typically, presodiation of HC could be conducted by directly contacting or cycling process [4, 32]. In addition, the presodiated process has been known as a widely applicable and simple approach in various practical full-cell assemblies to reduce capacity loss during long-cycling [33]. However, as can be seen in Table 1, the former process induced better ICE and slightly reduced the capacity while the latter process of HC destroyed the operation ability of the full-cell. It seems that the electrodes might be mechanically broken and contaminated by impurities from the deposition of electrolyte so that attention should be taken in conducting sodiation process to remain the quality of the electrode. Indeed, the presodiated HC could change not only the physical properties but also the capacity, resulting in an excessive N/P ratio that must be included to the full-cell assembly with presodiated anode. The aforementioned reasons contributed to the lower performance of presodiated-HC-anode full-cells compared to that of pure-HC-anode full-cells.

Using pure HC is beneficial for simplifying the cell assembly procedure, but the performance of the cell should be improved to meet the requirements of high energy density and long lifespan. Although a long charging time can enhance the number of charge release during discharge, thus improving the ICE of the cell, it is still not efficient in case the charging current is too low in the initial cycle (Figure 4, Table 2). Both charge modes M2 and M3 could not resolve the issue of the irreversible capacity related to Na loss of hard carbon anodes. The results, however, confirm a practical aspect that the charge/discharge regime also plays a role in improving the capacity, cycle stability, cycle life of the cell, etc. Briefly, charge/discharge regime optimization should be placed right after the choice of which type of HC anode to be introduced into full-cell assembly, this should be initially done to meet the highest energy and power density.

4. CONCLUSIONS

Full-cells with hard carbon (HC) || $NaFe_{0.45}Cu_{0.05}Co_{0.5}O_2$ were assembled and investigated for the performance. The cell using plain HC as anode displayed an initial capacity of 72.6 $mAh.g^{-1}$ but degraded rapidly over the cycle. Therefore, a presodiated process was applied to improve the low ICE of the HC anode. The HC anode pre-sodiated by cycling in half-cell enabled an increase in both initial Coulombic efficiency (from 53.0 % to 60.6 %) and capacity retention. Meanwhile, the full-cell assembled with sodium-contacted HC exhibited poor performance. The results demonstrated that the presodiated process improved the performance of the full-cell but the process should be optimized to prevent the negative electrode from structure degradation and side reactions. Besides, the capacity matching between the negative electrode and positive electrode must be adjusted when using the presodiated HC. The results also indicated that the charge/discharge regime also had an effect on the performance of the full-cell. The constant voltage charging improved the capacity while the low current charging initially destroyed the operation ability. This work is fancy but has provided us with many suggestions for maximizing the performance of sodium-ion full-cells.

Acknowledgments. This research is funded by Vietnam National University Ho Chi Minh City (VNU-HCM) under grant number C2020-18-10.

CRediT authorship contribution statement. Author 1: give idea, methodology and prepare and submit the manuscript. Author 2: analysis data. Author 3: synthesis of the material. Author 4: edit the manuscript. Author 5: edit the manuscript.

Declaration of competing interest. The authors declare that they have no known competing finacial interests or persional relationships that could have appeared to influence the work reported in this paper.

REFERENCES

1. Amine K., Kanno R. and Tzeng Y. - Rechargeable lithium batteries and beyond: Progress, challenges, and future directions, MRS Bull. **39** (2014) 395-401. https://doi.org/10.1557/mrs.2014.62.
2. Nayak P.K., Yang L., Brehm W., and Adelhelm P. - From lithium-ion to sodium-ion batteries: Advantages, challenges, and surprises, Angew. Chem. Int. Ed. **57** (2018) 102-120. https://doi.org/10.1002/anie.201703772.
3. Nitta N., Wu F., Lee J.T. and Yushin G. - Li-ion battery materials: present and future, Mater. Today **18** (2015) 252-264. https://doi.org/10.1016/j.mattod.2014.10.040.
4. Niu Y. B., Yin Y. X.. and Guo Y. G. - Nonaqueous sodium-ion full cells: Status, strategies, and prospects, Small. **15** (2019) 1900233.https://doi.org/10.1002/smll.201900233.
5. Hwang J. Y., Myung S. T. and Sun Y. K. - Sodium-ion batteries: present and future, Chem. Soc. Rev. **46** (2017) 3529-3614. https://doi.org/10.1039/C6CS00776G.
6. Yabuuchi N. , Kubota K. , Dahbi M. and Komaba S. - Research development on sodium-ion batteries, Chem. Rev. **114** (2014) 11636-11682. https://doi.org/10.1021/cr500192f.
7. Liu Q., Hu Z., Chen M., Zou C., Jin H., Wang S., Chou S. and DouS. - Recent progress of layered transition metal oxide cathodes for sodium-ion batteries, Small. **15** (2019) 1805381. https://doi.org/10.1002/smll.201805381.
8. Fang Y., Xiao L., Chen Z., Ai X., Cao Y. and Yang H. - Recent advances in sodium-ion battery materials, Electrochem. Energy Rev. **1** (2018) 294-323. https://doi.org/10.1007/s41918-018-0008-x.
9. Liu Y., Liu X., Wang T., Fan L. Z. and Jiao L. - Research and application progress on key materials for sodium-ion batteries, Sustain. Energy Fuels. **1** (2017) 986-1006. https://doi.org/10.1039/C7SE00120G.
10. Kim H., Kim H., Ding Z., Lee M.H., Lim K., Yoon G. and Kang K. - Recent progress in electrode materials for sodium-ion batteries, Adv. Energy Mater. **6** (2016) 1600943. https://doi.org/10.1002/aenm.201600943.
11. Wang H., Liao X. Z., Yang Y., Yan X., He Y. S., and Ma Z. F. - Large-scale synthesis of $NaNi_{1/3}Fe_{1/3}Mn_{1/3}O_2$ as high-performance cathode materials for sodium-ion batteries, J. Electrochem. Soc. **163** (2016) A565-A570. https://doi.org/10.1149/2.0011605jes.
12. Jeong M., Lee H., Yoon J. and Yoon W. S. - O3-type $NaNi_{1/3}Fe_{1/3}Mn_{1/3}O_2$ layered cathode for Na-ion batteries: Structural evolution and redox mechanism upon Na (de) intercalation, J. Power Sources. **439** (2019) 227064.

    https://doi.org/10.1016/j.jpowsour.2019.227064.

13. Zhou D., Huang W., Zhao F. and Lv X. - The effect of Na content on the electrochemical performance of the O3-type $Na_xFe_{0.5}Mn_{0.5}O_2$ for sodium-ion batteries, J. Mater. Sci. **54** (2019) 7156–7164. https://doi.org/10.1007/s10853-018-03277-8.

14. Yoshida H., Yabuuchi N. and Komaba S. - $NaFe_{0.5}Co_{0.5}O_2$ as high energy and power positive electrode for Na-ion batteries, Electrochem. Commun. **34** (2013) 60-63. https://doi.org/10.1016/j.elecom.2013.05.012.

15. Thorne J. S., Dunlap R. A., and Obrovac M. N. - Structure and electrochemistry of $Na_xFe_xMn_{1-x}O_2$ ($1.0 \leq x \leq 0.5$) for Na-ion battery positive electrodes, J. Electrochem. Soc. **160** (2013) A361-A367. https://doi.org/10.1149/2.058302jes.

16. Yabuuchi N., Kajiyama M., Iwatate J., Nishikawa H., Hitomi S., Okuyama, R., Usui R., Yamada Y. and Komaba S. - P2-type $Na_x[Fe_{1/2}Mn_{1/2}]O_2$ made from earth-abundant elements for rechargeable Na batteries, Nat. Mater. **11** (2012) 512-517. https://doi.org/10.1038/nmat3309.

17. Yao H. R., Wang P. F., Wang Y., Yu X., Yin Y. X., and Guo Y. G. - Excellent comprehensive performance of Na-based layered oxide benefiting from the synergetic contributions of multimetal ions, Adv. Energy Mater. **7** (2017) 1700189. https://doi.org/10.1002/aenm.201700189.

18. Mariyappan S., Marchandier T., Rabuel F., Iadecola A., Rousse G., Morozov A. V., Abakumov A. M., and Tarascon J. M. - The role of divalent (Zn^{2+}/Mg^{2+}/Cu^{2+}) substituents in achieving full capacity of sodium layered oxides for Na-ion battery applications, Chem. Mater. **32** (2020) 1657-1666. https://doi.org/10.1021/acs.chemmater.9b05205.

19. Yang L., Li X., Liu J., Xiong S., Ma X., Liu P., Bai J., Xu W., Tang Y., Hu Y. Y., Liu M. and Chen H. - Lithium-doping stabilized high-performance P2-$Na_{0.66}Li_{0.18}Fe_{0.12}Mn_{0.7}O_2$ cathode for sodium ion batteries, J. Am. Chem. Soc. **141** (2019) 6680-6689. https://doi.org/10.1021/jacs.9b01855.

20. Rong X., Qi X., Lu Y., Wang Y., Li Y., Jiang L., Yang K., Gao F., Huang X., Chen L., and Hu Y. S. - A new Tin-based O3-$Na_{0.9}[Ni_{0.45-x/2}Mn_xSn_{0.55-x/2}]O_2$ as sodium-ion battery cathode, J. Energy Chem. **31** (2019) 132-137.

    https://doi.org/10.1016/j.jechem.2018.05.019.

21. Li J., Wang J., He X., Zhang L., Senyshyn A., Yan B., Muehlbauer M., Cao X., Vortmann-Westhoven B., Kraft V., Liu H., Luerenbaum C., Schumacher G., Paillard E., Winter M., and Li J. - P2-Type $Na_{0.67}Mn_{0.8}Cu_{0.1}Mg_{0.1}O_2$ as a new cathode material for sodium-ion batteries: Insights of the synergetic effects of multi-metal substitution and electrolyte optimization, J. Power Sources. **416** (2019) 184-192.

    https://doi.org/10.1016/j.jpowsour.2019.01.086.

22. Van Hoang N., Minh Le N., Hue Phuong T., Van Man T., Nhan Thanh T. and My Loan Phung L. - Cu-Doped $NaCu_{0.05}Fe_{0.45}Co_{0.5}O_2$ as promising cathode material for Na-ion batteries: Synthesis and characterization, J. Solid State Electrochem. **25** (2020) 1-9. https://doi.org/10.1007/s10008-020-04851-4.

23. Chen X., Zheng Y., Liu W., Zhang C., Li S., Li J. - High-performance sodium-ion batteries with a hard carbon anode: transition from the half-cell to full-cell perspective, Nanoscale. **11** (2019) 22196-22205. https://doi.org/10.1039/C9NR07545C.

24. Xie F., Xu Z., Guo Z., and Titirici M.-M. - Hard carbons for sodium-ion batteries and beyond, Prog. Energy. **2** (2020) 042002. https://doi.org/10.1088/2516-1083/aba5f5.

25. Hou H., Qiu X., Wei W., Zhang Y., and Ji X. - Carbon anode materials for advanced sodium-ion batteries, Adv. Energy Mater. **7** (2017) 1602898.
26. Jamesh M.I. and Prakash A.S. - Advancement of technology towards developing Na-ion batteries, J. Power Sources. **378** (2018) 268-300.

    https://doi.org/10.1016/j.jpowsour.2017.12.053.
27. Kubota K., Asari T., Yoshida H., Yaabuuchi N., Shiiba H., Nakayama M., and Komaba S. - Understanding the structural evolution and redox mechanism of a $NaFeO_2$-$NaCoO_2$ solid solution for sodium-ion batteries, Adv. Funct. Mater. **26** (2016) 6047-6059. https://doi.org/10.1002/adfm.201601292.
28. Irisarri E., Ponrouch A., and Palacin M. R. - Review-Hard carbon negative electrode materials for sodium-ion batteries, J. Electrochem. Soc. **162** (2015) A2476-A2482. https://doi.org/10.1149/2.0091514jes.
29. Chen G., Liu Z., and Su H. - An optimal fast-charging strategy for lithium-ion batteries via an electrochemical-thermal model with intercalation-induced stresses and film growth, Energies. **13** (2020) 2388. https://doi.org/10.3390/en13092388.
30. Wang Z., Wang Y., Rong Y., Li Z., and Fantao L. - Study on the optimal charging method for lithium-ion batteries used in electric vehicles, Energy Procedia. **88** (2016) 1013-1017. https://doi.org/10.1016/j.egypro.2016.06.127.
31. Wu X., Hu C., Du J., and Sun J. - Multistage CC-CV charge method for Li-ion battery, Math. Probl. Eng. **2015** (2015) 1-10. https://doi.org/10.1155/2015/294793.
32. Zhang X., Fan C., and Han S. - Improving the initial Coulombic efficiency of hard carbon-based anode for rechargeable batteries with high energy density, J. Mater. Sci. **52** (2017) 10418-10430. https://doi.org/10.1007/s10853-017-1206-3.
33. Wang H., Xiao Y., Sun C., Lai C., and Ai X. - A type of sodium-ion full-cell with layered $NaNi_{0.5}Ti_{0.5}O_2$ cathode and pre-sodiated hard carbon anode, RSC Adv. **5** (2015) 106519-106522. https://doi.org/10.1039/C5RA21235A.